Journal of Luminescence 250 (2022) 119070

Contents lists available at ScienceDirect

Journal of Luminescence

journal homepage: www.elsevier.com/locate/jlumin

Full Length Article

A systematic multi-technique comparison of luminescence characteristics of two reference quartz samples

Christoph Schmidt [a], Alicja Chruścińska [b,*], Mauro Fasoli [c], Magdalena Biernacka [b], Sebastian Kreutzer [d,e,f], Georgios S. Polymeris [g], David C.W. Sanderson [h], Alan Cresswell [h], Grzegorz Adamiec [i], Marco Martini [c]

[a] University of Lausanne, Institute of Earth Surface Dynamics, Géopolis, Lausanne, Switzerland
[b] Institute of Physics, Faculty of Physics, Astronomy and Informatics, Nicolaus Copernicus University in Toruń, ul. Grudziądzka 5, 87-100, Toruń, Poland
[c] Dipartimento di Scienza dei Materiali, Università degli Studi di Milano-Bicocca, Milan, Italy
[d] Geography & Earth Sciences, Aberystwyth University, Aberystwyth, Wales, United Kingdom
[e] Archéosciences Bordeaux, UMR 6034, CNRS - Université Bordeaux Montaigne, Pessac, France
[f] Institute of Geography, Heidelberg University, Heidelberg, Germany
[g] Institute of Nanoscience and Nanotechnology, National Centre for Scientific Research "Demokritos", Athens, Greece
[h] Scottish Universities Environmental Research Centre, Rankine Avenue, East Kilbride, United Kingdom
[i] Institute of Physics - Centre for Science and Education, Division of Geochronology and Environmental Isotopes, Silesian University of Technology, Konarskiego, 22B, 44-100, Gliwice, Poland

ARTICLE INFO

Keywords:
Luminescence dating
Quartz
Reference samples
TL
OSL
LM-OSL
TM-OSL
RL
TR-OSL

ABSTRACT

Further developments in luminescence dating, dosimetry and temperature-sensing require a deep understanding of luminescence processes and their driving parameters. Natural quartz is one of the most widely used minerals for these purposes. Still, poor reproducibility of results often hampers comparability and credibility from findings in the literature. We identified the lack of suitable natural reference samples as a pivotal problem impeding significant progression. Ideally, basic investigations involve several laboratories working on well-characterised reference quartz samples with different characteristics. Investigations should include multiple complementing methods to analyse luminescence properties and mineralogical and geochemical composition.

Here, we present such a multi-technique luminescence comparison of two natural quartz samples. Next to the recently introduced Fontainebleau (FB) reference quartz, we propose another reference sample derived from the 'Silver Sands of Morar' (lab code 'MR'; Scotland, UK). Our experiments confirm that both quartz samples behave fundamentally different in terms of signal composition and sensitivity. The comparative characterisation of both samples targeted electron traps via thermoluminescence (TL) and optically stimulated luminescence (OSL) techniques and luminescence centres via radioluminescence and time-resolved OSL spectrometry. In summary, we conclude that all observed differences are likely the results of divergent defect concentrations rather than variances in defects' composition (nature). The measurement data of our study are accessible open-access for inspection by others.

1. Introduction

In luminescence dating, dosimetry and temperature-sensing, we exploit phenomena of light production in natural and synthetic isolators and semi-conductors involving complex physical mechanisms. Quartz, as a natural material, has a stable crystal structure that is relatively free from impurities compared to other minerals (e.g., Refs. [1,2]). Still, samples' luminescent properties differ significantly in the spectrum of charge-trapping states and the emission spectrum, which depend on the presence of intrinsic defects and substitutional and/or interstitial trace impurities. The fact that sediments, usually a mixture of grains of various origins, are frequently used in geochronology and related applications render systematic research even more complicated. The processes taking place in the quartz crystal upon external stimulation (heating, illumination, irradiation) and after that, ultimately triggering the signal we use to determine the equivalent dose or trap saturation

* Corresponding author.
E-mail address: alicja@fizyka.umk.pl (A. Chruścińska).

https://doi.org/10.1016/j.jlumin.2022.119070
Received 9 March 2022; Received in revised form 23 May 2022; Accepted 10 June 2022
Available online 13 June 2022

states, cannot be regarded as being isolated from each other. Hence, understanding these mechanisms, their interaction and determining the basic physical parameters governing these processes is crucial for the accuracy and precision of the final result.

A vast literature body presents basic physical parameters of charge-trapping states responsible for luminescence (for an overview, cf. [3,4]). However, it is challenging to compile a list of such parameters unequivocally attributed to quartz of various types and origins. Parameters reported in numerous studies usually concern a limited number of samples instead of parallel experiments under the same conditions for a larger set of samples. Ideally, samples are tested in many experiments against a so-called reference sample with reproducible and well-known characteristics. This requires a collection of reference samples and a database of results obtained for these samples. If carefully extended and supplemented with the analysis of defects in the samples by complementary methods, such data will significantly advance our knowledge about the trapping sites and processes in quartz responsible for the luminescence signals used in trapped-charged applications. Our contribution is an attempt towards that aim as joint work in multiple laboratories addressing fundamental questions of luminescence production in quartz by systematic multi-technique comparison of reference quartz samples.

For this work and, hopefully, for further efforts to extend the sample list, we consider a quartz sample as a reference sample if it meets the following criteria:

- The sample is available to a larger number of laboratories in larger quantities (>500 g) located securely in a declared place,
- the preparation and purification methods of the reference sample are described in detail,
- mineralogical and elemental composition analyses have confirmed the purity of the quartz,
- the sample is the subject of many works, where it is declared under its unambiguously defined name so that it is easy to track published results for this sample,
- the measurement description in the publications presenting the sample contains all necessary details allowing the repetition of analogous measurements and the direct comparison of their results with other well-characterized or unknown samples.

We present several parallel experiments for two samples of different origins, which we propose as reference samples. The first one, FB (Fontainebleau), was thoroughly described earlier by Kreutzer et al. [5]. It was already used in an interlaboratory comparison of trap parameters measured for the 110 °C thermoluminescence (TL) peak involving eight laboratories. This study showed how significant the effect of experimental conditions is on the derived parameters' values, even when the measurements are carried out with the same type of luminescence reader [6]. The FB sample has further served as a reference in studying time-resolved optically stimulated luminescence (TR-OSL) in the nanosecond time domain performed for a broader range of quartz samples of various origins [7]. The high intensity of the fast OSL component of this sample favours works aiming at an experimental separation of this component from the slower components using the thermally modulated OSL (TM-OSL) method with a 620 nm stimulation light [8,9]. Finally, FB was examined in experiments centring on the UV reversal effect and quenching processes studied employing the quartz UV radioluminescence signal and on the dose-rate dependence of this emission [10–12]. The second sample, MR (Morar), was collected from the banks of the Morar River in Scotland, UK. The first screening showed noticeably different luminescence properties than sample FB; hence, it represents a good candidate for expanding the sample set.

In this paper, the TL of sample MR was recorded to provide a first insight into the difference between both samples in the nature and concentration of traps responsible for the signal recorded in the usually targeted UV emission window. OSL analyses encompassed linear-modulation OSL (LM-OSL) and thermally-modulated OSL (TM-OSL) and allowed a comparison of the optically active traps in both samples. Furthermore, to characterize the luminescence centres involved in OSL and TL production, we recorded TR-OSL and radioluminescence (RL) spectra.

2. Samples

2.1. Sample origin and genesis

The Fontainebleau (FB) sample originates from the coastal palaeodune system (Oligocene Fontainebleau Sandstone Formation, France) from the time of the last marine intrusion into the Paris Basin (the Stampian Sea) ~35 Ma ago. It contains quartz grains originating from plutonic, volcanic, and metamorphic rocks. Further details are given in Kreutzer et al. [5].

The Morar (MR) sample is from ~8 ka to 9 ka old deposits (the 'Silver Sands of Morar') on the banks of an active estuary (56° 57′ 40″N, 5° 49′ 25″W), reworked intensely by fluvial and marine processes. It represents a mixture of grains mostly from metasedimentary rocks (mainly quartz and feldspar-bearing psammites) from the Moinian Morar Formation with a minor contribution from hornblendic and feldspathic gneiss [13]. Several kilograms of material were taken under daylight conditions in March 2017.

2.2. Sample preparation

The preparation of sample FB is described in detail in Kreutzer et al. [5]. For MR, sieved material within the grain size range 150–250 μm was subject to magnetic separation to remove heavy minerals from the quartz and feldspar fraction (for details, see Ref. [5]). The non-magnetic fraction still contained some mica, and it was then further purified by froth flotation. This procedure includes a 30 min wash in 1% HF to softly attack the grains' surfaces, then they were mixed with a few drops of eucalyptus oil and suspended in foam produced with lauryl amine (N-dodecylamine) by a machine usually employed for enriching beverages with carbon dioxide. This treatment causes the feldspar and mica grains to coagulate and float on top of the solution while the quartz grains remain at the bottom. The contaminants can then easily be decanted. While part of the so-obtained material was retained in its current state, one further subsample was etched in 40% HF for 40 min at 25.8 °C (replacing the acid after half of the etching duration) while stirring manually and using ultrasonics followed by re-sieving (100 μm) after neutralisation and drying from acetone at 50 °C. Another subsample was etched in fluorosilicic acid (H_2SiF_6) for 10 days. These two acid treatments aimed at removing minor feldspar contamination in the samples detected by IRSL measurements. From a starting mass of 20.8 g, about 12 g were left after HF etching, while about 18.6 g remained from 20.5 g starting material for etching in H_2SiF_6. The following investigations were carried out on the HF-etched fraction only. Preparation procedures applied in the case of both reference quartz samples are compared in Table 1.

Table 1
Comparative sample preparation scheme for the two reference quartz samples.

Treatment	FB[a]	MR
Sieving to 150–250 μm	✓	✓
Magnetic separation to remove heavy minerals	✓	✓
Flotation to remove mica and feldspars		✓
Etching in 40% HF for 40 min to dissolve feldspar, re-sieving (100 μm)		✓
Annealing at 490 °C for 30 min	✓	

[a] FB underwent the chemical washing and density separation by the supplier (MERCK); details are not available.

2.3. Sample purity investigations

Scanning electron microscopy in low-vacuum backscatter mode was used with semi-quantitative element measurements by X-ray fluorescence (XRF) spot analyses to test for sample purity and characterise non-quartz constituents. XRF on >20 grains detected no impurities, but especially for the smaller grains (<90 μm) that were analysed in addition to the target grain size range, we found minor adherents on the grains rich in Cu and Ni. Detailed findings for the FB sample are summarised in Ref. [5]. In summary, both reference samples consist of >99% SiO_2.

3. Equipment and measurement details

3.1. TL, TM-OSL and LM-OSL measurements

TL, TM-OSL and LM-OSL measurements were carried out using a Risø TL/OSL-DA-12 reader (after a refurbishment; hereafter referred to as system 1) equipped with an EMI 9235QA photomultiplier and the combination of a 7.5 mm Hoya U-340 and a 2 mm Chroma 79–340 bandpass filter (main transmission band at 335–345 nm) for luminescence detection, and with an external unit for optical stimulation. The unit allowed the stimulation with five LED modules made of single high-power LEDs (3 W, Bridgelux, Inc.). The maxima of their spectral bands are 620 nm, 580 nm, 530 nm, 490 nm and 470 nm. They are directly integrated with an optical adapter inserted into the Risø reader instead of the earlier halogen lamp. For some of the TL and TM-OSL measurements, a Risø TL/OSL-DA-20 (hereafter referred to as system 2) reader was used. The signal was detected by an EMI 9235QB photomultiplier and a 7.5 mm Hoya U-340 bandpass filter. Optical stimulation was performed using the above-mentioned LEDs modules with wavelengths 620 nm and 530 nm. The heating during the TL reading was performed at 2 K s^{-1} in an argon atmosphere. Irradiation was done using a $^{90}Sr/^{90}Y$ β-source with a dose rate of ~0.03 Gy s^{-1} or ~0.1 Gy s^{-1} for systems 1 and 2, respectively. Figure captions contain further information about the used equipment.

For LM-OSL [14], LED modules facilitated stimulation at 470 nm (FWHM = 25 nm) and 530 nm (FWHM = 25 nm), with maximum photon flux densities of 4.9×10^{17} cm^{-2} s^{-1} and 1.7×10^{17} cm^{-2} s^{-1} at the sample position, respectively. The stimulation light intensity was linearly ramped from 0% to 100% over 5000 s and at 125 °C read-out temperature. The grains were deposited on stainless steel discs delivered by Risø using silicon spray and a 6 mm diameter aliquot mask. Two aliquots of each sample were used. The weights of the samples are given in the figure captions presenting the relevant data.

3.2. TR-OSL measurements

TR-OSL analyses were carried out with a Freiberg Instruments lexsyg research reader [15], using green LEDs (525 ± 25 nm, photon flux density ~1.58×10^{17} cm^{-2} s^{-1} at the sample position) for stimulation with pulses of 10 μs duration (on-time) and an off-time of 290 μs in between the pulses. The dwell time was set to 10 μs, and 10^7 scans were recorded per measurement. Spectra were recorded at room temperature (~25–30 °C) after a regeneration dose of 19 Gy (FB) or 310 Gy (MR) delivered by a $^{90}Sr/^{90}Y$ β-source (dose rate ~0.04 Gy s^{-1}) and without preheating (cf. [16]). Signals were recorded with a Hamamatsu H7360-02 photomultiplier after passing through the combination of a 3 mm Schott BG-3 glass filter and a Delta BP 365/50 interference filter. Three aliquots were measured for each sample. TR-OSL spectra were fitted to several exponential decays using the function `fit_OSLLifeTimes()` [7] as part of the R [17] package 'Luminescence' [18,19].

3.3. RL measurements

Radioluminescence (RL) measurements were carried out at room temperature (RT) using a homemade apparatus featuring, as a detection system, a back-illuminated UV-enhanced charge-coupled device (CCD) (Jobin–Yvon) coupled to a Triax 180 spectrograph (Jobin–Yvon). RL excitation was obtained by X-ray irradiation through a Be window, using a Philips 2274 X-ray tube, with a tungsten target, operated at 20 kV and 20 mA (dose rate at sample position ~0.33 Gy s^{-1}). All the spectra were corrected, taking into account the sensitivity of the detection system.

4. Results

4.1. TL

TL curves measured for both samples are presented in Fig. 1. Two curves are shown for each sample, relating to regenerative doses of 150 Gy and 300 Gy. Shapes of TL curves measured after the same dose are reproducible from aliquot to aliquot of a sample.

The TL intensity is significantly higher for FB than for MR in the whole temperature range, except around 250 °C. The difference is more significant for temperatures >100 °C. Whereas the 110 °C TL peak, detected here at 80 °C because of the low heating rate, is about twice as intense in sample FB as in MR, the signal in the high-temperature region, depending on the TL peak, is from 4 to 12 times greater in sample FB. Simultaneously, in this range, we observed significant differences in the shape of TL curves between both samples. A peak at 165 °C, like the one at 250 °C, is apparent in the TL of sample MR but not at all in the curve of the other sample. Conversely, the peak at 185 °C is very high in sample FB but does not seem to be present in the TL of sample MR. For a heating rate of 2 K s^{-1}, the TL peak originating from the traps responsible for the fast OSL component is detected at ~285 °C. This peak is observed in TL of sample FB but is relatively low in the case of sample MR. The high TL intensity of sample FB in this region fits well with the strong fast OSL component in this sample.

The TL curve shapes of both samples change with dose, as shown in Fig. 1. From 150 Gy to 300 Gy, the TL signal of sample MR increases by a factor of three (supralinear dose-response) between 150 °C and 200 °C. In the same temperature range, FB shows a sublinear dose-response. Between 200 °C and 300 °C, the TL signal of sample FB increases with dose quicker than in sample MR, whereas, above 300 °C, the tendency reverses again. Since these measurements were done on the same aliquot, the role of potential sensitivity changes affecting TL intensity levels remains unclear at this stage of the initial TL screening. However, our observations indicate that the concentrations of the defects

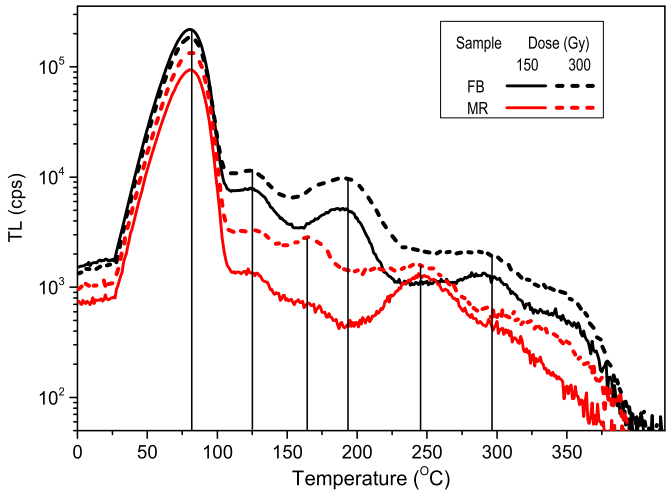

Fig. 1. TL curves for one aliquot each of the FB (black) and MR (red) sample, measured promptly after irradiation with doses of 150 Gy (solid line) or 300 Gy (dashed line) after background subtraction. (System 1, sample masses: FB – 4.8 mg, MR – 4.8 mg).

responsible for the individual electron traps in the samples are different.

The discrepancies in TL dose-response between the samples indicate that competition processes between traps and recombination centres occur differently. Especially the latter can be expected when looking at the sensitivity changes of the 110 °C peak with cumulative dose. The procedure used for the sensitivity investigation in freshly prepared aliquots of both samples included the following steps: (1) initial heating to 500 °C, (2) irradiation (8 Gy), (3) TL to 250 °C with 2 K s^{-1}, (4) repeat steps 2–3 for 75 times, resulting in a cumulative dose range of 8–600 Gy. As shown in Fig. 2, both samples' 110 °C TL peak sensitivity behaviour differs fundamentally. The sensitivity in sample FB for cumulative doses <60 Gy quickly decreases (Fig. 2a, c). After reducing by 25%, it increases slightly and then drops again slowly for doses >200 Gy and at 600 Gy, reaching a value ~35% lower than the initial sensitivity. Contrary, in the MR sample, the sensitivity increases by 120% for doses <300 Gy, forming a plateau before decreasing slowly, reaching a sensitivity at the end of the experiment ~5% lower than the maximum at 300 Gy (Fig. 2b and c).

This experiment is very similar to tests by Friedrich et al. [12] on a subsample of the FB quartz (FB2A, their Fig. 2). Friedrich et al. [12] also reported a decrease of the 110 °C peak of the FB sample with dose and were able to model this pattern (Friedrich et al. [12], their Fig. 7) using their quartz model adapted to simulate UV-radiofluorescence [20]. Compared to the Bailey [21] model, Friedrich et al. [20] modified the parameters for the reservoir centre R1 and the deep electron trap. We ran simulations using the quartz model by Friedrich et al. [20] for the dose-response sequence detailed above to test whether the model can also mimic our findings for both samples. For the simulation, we used the R [17] package 'RLumModel' ([22]; v0.2.10) (see supplement for applied code and results). As expected, the model output is qualitatively similar for the FB measurements, with a quenched 110 °C TL peak with cumulated dose. However, it failed to depict the observations for the MR sample, unless the concentration R1 (parameter N_{R1}) was decreased. The changed concentration of non-radiative reservoir centres might be explained by the heat treatment of the FB sample (490 °C stabilised over 30 min), potentially increasing the accessible concentration of such centres, thus allowing for a higher competition with the L centre. Further details and tests must remain subject to future studies. However, we could generally simulate both behaviours with existing models, which is reassuring.

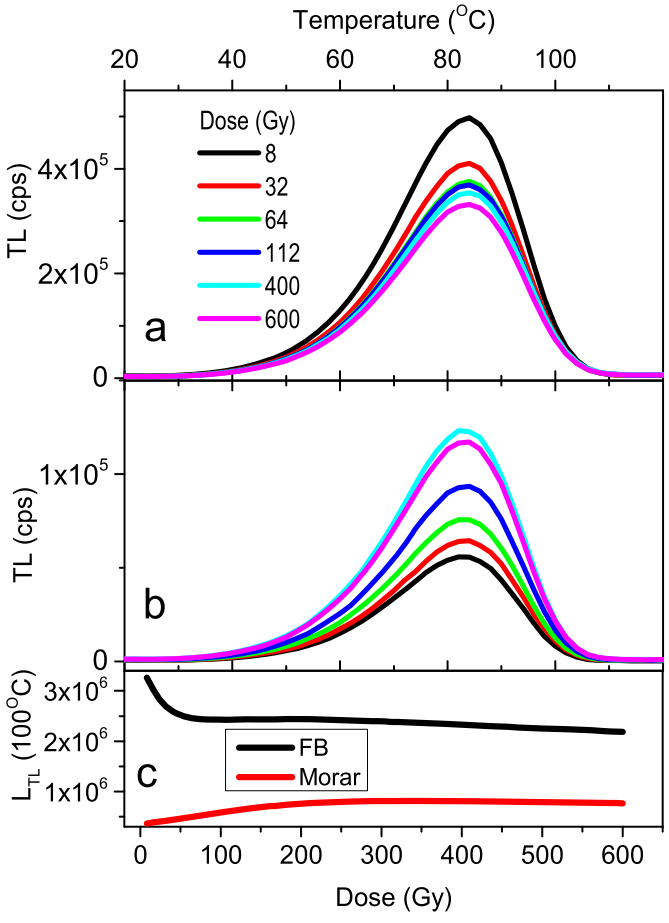

Fig. 2. Sensitivity changes of the 110 °C TL peak resulting from the protocol described in Section 4.1 (a) Representative TL glow curves for sample FB, cumulative dose as indicated by the colour code; (b) Representative TL glow curves for sample MR, cumulative dose as indicated by the colour code in (a); (c) Comparison of the intensities (sum of counts in the range 78–90 °C) of both samples as a function of cumulative dose. Note that (a) and (b) share the same (temperature) axis, while (c) has a different (dose) axis. (System 2, sample masses: FB – 4.3 mg, MR – 3.9 mg).

It is interesting to see how the TL signal changes when one widens the detection window, removing the U-340 filter. The spectral window is then limited by the quantum efficiency of the photomultiplier, which allows for shifting the limit of the detection window towards lower energies. Fig. 3 compares the TL curves obtained after preheating to 260 °C with and without the U-340 filter. As removing the filter results in a significant enhancement of the TL for both samples, the curves measured with the filter are shown after multiplying them by 10. The increase is stronger above 300 °C. Below 300 °C, TL measured without the filter is 12 times more intense for sample FB and 10 times more intense for sample MR than TL detected through the filter and, above 300 °C, these factors amount to ~23 and ~25, respectively. This renders the shapes of TL curves observed in the two detection windows noticeably different.

4.2. OSL

The OSL signal of the samples was investigated using LM-OSL, TM-OSL and TR-OSL. The influence of the partial bleaching of the fast(er) components in the TM-OSL method on the signal observed by the LM-OSL method was tested to correlate the components observed in both measurements.

4.2.1. LM-OSL

Fig. 4 displays the results of LM-OSL measurements with stimulation wavelengths of 470 nm and 530 nm. All curves show two separated bell-

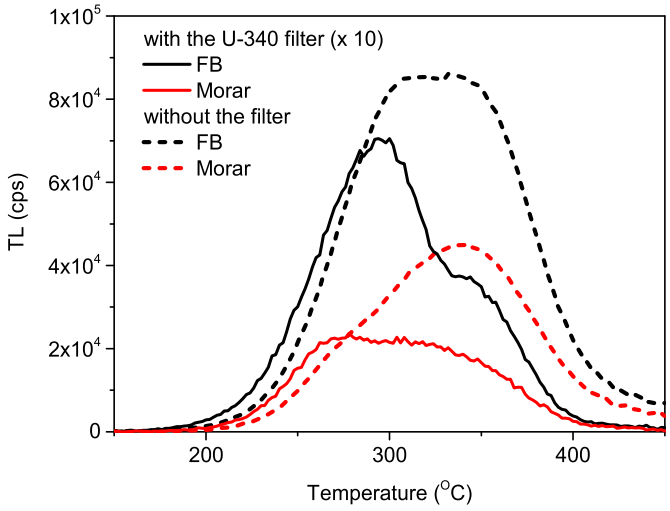

Fig. 3. Comparison of TL curves obtained for the same conditions and aliquots of samples FB and MR with and without the U-340 filter. The curves were measured with a heating rate of 2 K s^{-1} after irradiation with a dose of 300 Gy and preheat to 260 °C. (System 2, sample masses: FB – 4.8 mg, MR –_4.8 mg).

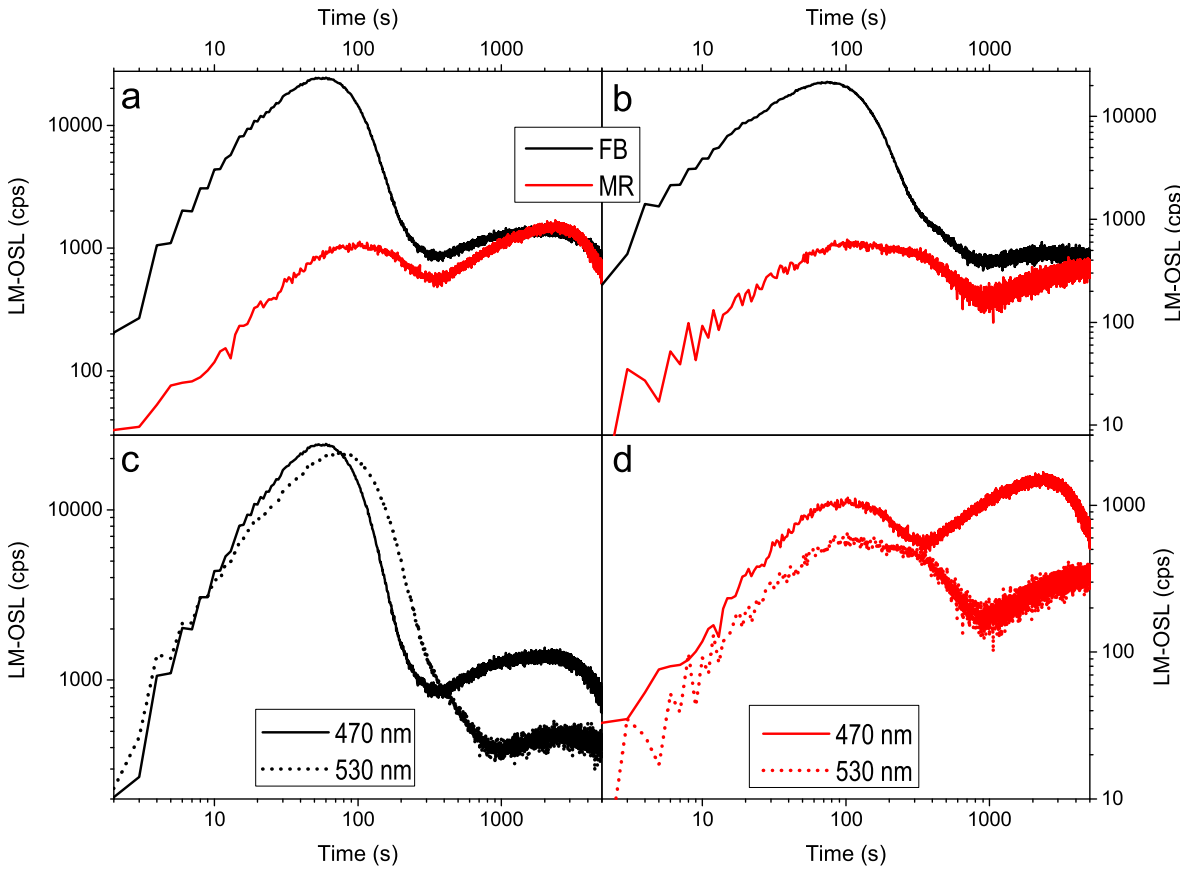

Fig. 4. LM-OSL curves of samples FB and MR measured at 125 °C for 5000 s of linearly ramped optical stimulation with 470 nm (a) and 530 nm (b), following a dose of 150 Gy and preheat to 250 °C; comparison of LM-OSL curves obtained for different wavelengths for sample FB (c) and MR (d). (System 1, sample masses: FB – 4.8 mg, MR – 4.8 mg).

shaped maxima: nevertheless, the full width at half maximum (FWHM) along with the corresponding LM-OSL peak shape methods [23] indicate that this LM-OSL decay curve is a composite, with the first maximum being created by the fast and medium (more clearly visible in sample MR) OSL components while the second by the slow components. It is essential to note that the position of the maximum intensity of one LM-OSL component is directly correlated to the corresponding optical cross-section, as the latter depends on t_m^{-2} (t_m = time of maximum signal intensity; [23,24]). The LM-OSL curves of both samples differ in shape and intensity in the initial 300 s. The relative differences in signal intensity of the fast component in sample FB and the first LM-OSL maximum of sample MR are significant. In contrast, intensities for both samples are comparable for the second LM-OSL maximum.

Fig. 4c and d compare LM-OSL curves stimulated at 470 nm and 530 nm. The two bell-shaped maxima in each LM-OSL curve, in both samples, behave differently with the change of stimulation wavelength (Fig. 4c and d). While a clear difference is observed in the position, and also in the shape, of the second maximum for stimulation wavelengths of 470 nm and 530 nm (for sample FB, Fig. 4c, shift towards longer times by about 500 s), the shift of the first maximum is much less pronounced. This peak change is more pronounced in the LM-OSL curves of sample MR where the fast component does not dominate the signal at shorter stimulation times. Nevertheless, as the signals are a composite, differences in either shape or position corresponding to the maximum intensity might reflect the different bleaching characteristics of each component.

Additionally, we compared TL curves after heating to 250 °C and subsequent LM-OSL measurements and TL curves measured after identical thermal treatment but without LM-OSL readout. The difference curve presents the part of the TL signal bleached by optical stimulation

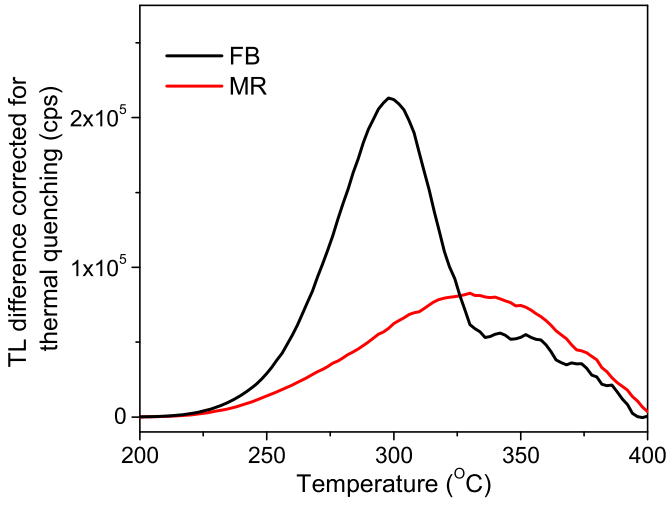

Fig. 5. The difference between TL curves measured after a dose of 150 Gy, preheat to 250 °C and holding the sample at 125 °C for 5000 s, and the TL curve after identical dose and preheat, and 470 nm LM-OSL at 125 °C for 5000 s. The curves are measured with a heating rate of 2 K s^{-1} and corrected for thermal quenching, a strong effect diminishing luminescence in quartz above 150 °C (e.g., Refs. [29–31]). Taking into account the similarity of the emission spectra for both samples and the same detection window used in measurements, the thermal quenching parameters, which were determined previously for sample FB [12] were used for both samples. (System 1, sample masses: FB – 4.8 mg, MR – 4.8 mg).

(here 5000 s at 125 °C; Fig. 5). The traps feeding the TL signal in a wide temperature range from 250 °C to 400 °C are depopulated by light exposure at 470 nm. Considering that the same traps contribute (in general) to TL and OSL, it is prominent that the traps within the temperature range 225–375 °C contribute to the entire blue OSL signal. In the case of sample FB, in the broad TL band, an intense peak at 300 °C (at 325 °C for a heating rate of 5 K s^{-1}) stands out, which is, according to Ref. [25], responsible for the fast OSL component. The presence of this peak in the FB sample signal is consistent with the observation of the intensive fast OSL component in this sample. Apart from this dominant TL peak, the rest of the signal of sample FB and the entire curve in the case of the MR sample constitute a wide, blurred band in which it is difficult to correlate TL peaks with individual types of traps. This feature stands in excellent agreement with previous studies that have provided experimental evidence that (i) one TL peak can feed more than two LM-OSL components and (ii) two different TL peaks can contribute to the same OSL component [26–28].

4.2.2. TM-OSL

TM-OSL is the OSL obtained by optical stimulation with constant wavelength while linearly ramping the sample temperature [32,33]. The method exploits the dependency of the optical cross-section (OCS) on the temperature to separate the signal from various types of traps more effectively. If the light of a longer wavelength is used for stimulation, differences between the OCSs of different traps are more significant, and the OCS increases more dynamically with temperature. Only traps most sensitive to the stimulating light are emptied for a suitable wavelength. Additionally, the OCS of these traps continuously enlarges with heating, reducing the time necessary for emptying the investigated traps and protecting other traps not intended to be emptied. The specific shape of TM-OSL curves can help determine the trap's optical depth and the electron-phonon coupling parameters [30]. During TM-OSL measurement, traps are both thermally and optically activated. Hence, TM-OSL measurements are carried out in the temperature range where thermal activation is negligible.

TM-OSL is suited for investigating deep traps after depopulating shallower traps. Both reference samples were measured after preheating, which was supposed to empty most of the traps shallower than those responsible for the fast OSL component. Chruścińska and Szramowski [9] showed that the fast OSL component in quartz could be measured using stimulation at 620 nm. Therefore, separating individual quartz OSL components with TM-OSL should start with stimulation at $\geq$ 620 nm.

To demonstrate the fundamental differences in the TM-OSL signal of both samples, five stimulation wavelengths, 620 nm, 580 nm, 530 nm, 490 nm, and 470 nm, were used for sequential TM-OSL measurements after initial irradiation and preheating to 260 °C. In the following, we will use subscripts to denote TM-OSL stimulation wavelengths (e.g., TM-OSL_{620}). All TM-OSL curves were measured to 240 °C (1 K s^{-1}) during heating. Then the sample was cooled down, and a subsequent TM-OSL measurement was performed. Table 2 lists the protocol used in the experiment, and Fig. 6 shows its results.

The biggest difference between the two reference samples is their TM-OSL_{620}. The luminescence of sample FB is about 100 times stronger than that of sample MR. This finding is consistent with the results of the LM-OSL measurement (Sec. 4.2.1), where the first "bell" of the LM-OSL curve in sample MR shows a low intensity. Still, the TM-OSL results exhibit that the fast component, although having a considerably lower intensity than sample FB, is present in the OSL of sample MR.

At shorter wavelengths, signal intensity differences (FB $\gg$ MR) are much more minor, and the curve shapes of both samples differ. For TM-OSL at 530 nm, a strong, slowly decaying part dominates in the TM-OSL of sample FB, whereas it forms a peak for sample MR. TM-OSL_{490} and TM-OSL_{470} display similar differences. For the latter, we observed a faster initial decay for sample FB.

After measuring the TM-OSL_{620} curve for the fast component, the repetition of the stimulation with the same wavelength led to a weak signal, unlike the first TM-OSL curve. This proves that the fast component was efficiently bleached during the first TM-OSL_{620} run. Moreover, a similar curve of lower intensity is observed in both samples for repeated TM-OSL_{580} measurements.

A stronger TM-OSL signal is observed again during the subsequent stimulation at 530 nm. A repetition of TM-OSL_{530} results in a weak and broad signal with a maximum of around 160 °C. For sample FB, the maximum is preceded by slow decay. TM-OSL_{490} led only to slightly increased intensities of the curve measured a step before but resulted in significantly higher intensity for TM-OSL_{470}.

The curve shapes of both samples in the first TM-OSL_{470}, albeit less and less intense, materialize in subsequent repetitions of TM-OSL_{470} measurements. Such a behaviour relates to a measurement in which only part of the OSL traps is emptied, and the temperature range in which these traps are effectively thermally emptied is significantly above TM-OSL's detection temperature range [32]. However, this mechanism unlikely causes the repetition of the initial rapid decay, visible in the TM-OSL curves of sample FB. It seems that here some unknown charge transfer effects are responsible for refilling the trap formerly emptied at the start of the optical stimulation (cf. [34]). A thermal transfer effect seems implausible due to the prolonged optical stimulation throughout the TM-OSL measurement that must have emptied particularly the traps responsible for the signal at the beginning of the stimulation.

The broad curve maximum around 160 °C seen in the TM-OSL_{530} repetitions is present in the MR and the FB samples. This signal must be related to the optical release of charges from traps responsible for the slower components.

Fig. 7 compares the fast OSL component and the next component in terms of decay rate. The experimental parameters to obtain TM-OSL_{620} and TM-OSL_{530} were selected to minimise peak-shape deformation: the preheat after irradiation and the heating inTM-OSL_{620} were continued to 290 °C. TM-OSL_{620} was repeated to empty the traps responsible for the fast component prior to TM-OSL_{530}. The slowly decaying initial part of the TM-OSL_{530} curve of sample FB seen in the previously described experiment, where heating stopped at 240 °C (Fig. 6b), disappeared after such a treatment. Therefore, it can be supposed that this signal is related to traps that are thermally depleted between 240 °C and 290 °C.

4.2.3. Correlation of components isolated in LM-OSL and TM-OSL measurements

The possibility of separating OSL components of different optical bleachability in TM-OSL experiments allows correlating these components with the ones extracted from LM-OSL measurements. A successive series of four TM-OSL and LM-OSL measurements were carried out for two aliquots of each sample to observe the changes in the LM-OSL curve caused by the prior measurement of TM-OSL components.

To identify in LM-OSL curves the effect of optical stimulation as part of the TM-OSL sequence, we compared the LM-OSL curve obtained after the TM-OSL with the one measured **after the same thermal treatment** but without optical stimulation (protocol Table 3). Curve LM_2 was obtained after bleaching the fast component with TM-OSL_{620} and curve LM_4 after TM-OSL_{530} (medium component). We repeated TM-OSL_{530} to ensure that the traps responsible for the last component were emptied. Curves LM_1 and LM_3 represent reference curves for LM_2 and LM_4,

Table 2
Protocol used in the TM-OSL experiment whose results are presented in Fig. 6.

Step	Treatment
1	Irradiation (300 Gy)
2	Preheat up to 260 °C (1 K s^{-1})
3	TM-OSL - optical stimulation at λ_i[a], heating to 240 °C with 1 K s^{-1}
4	Back to step 3

[a] λ_i was chosen successively: 620 nm, 620 nm, 580 nm, 530 nm, 530 nm, 490 nm, 470 nm, 470 nm, 470 nm.

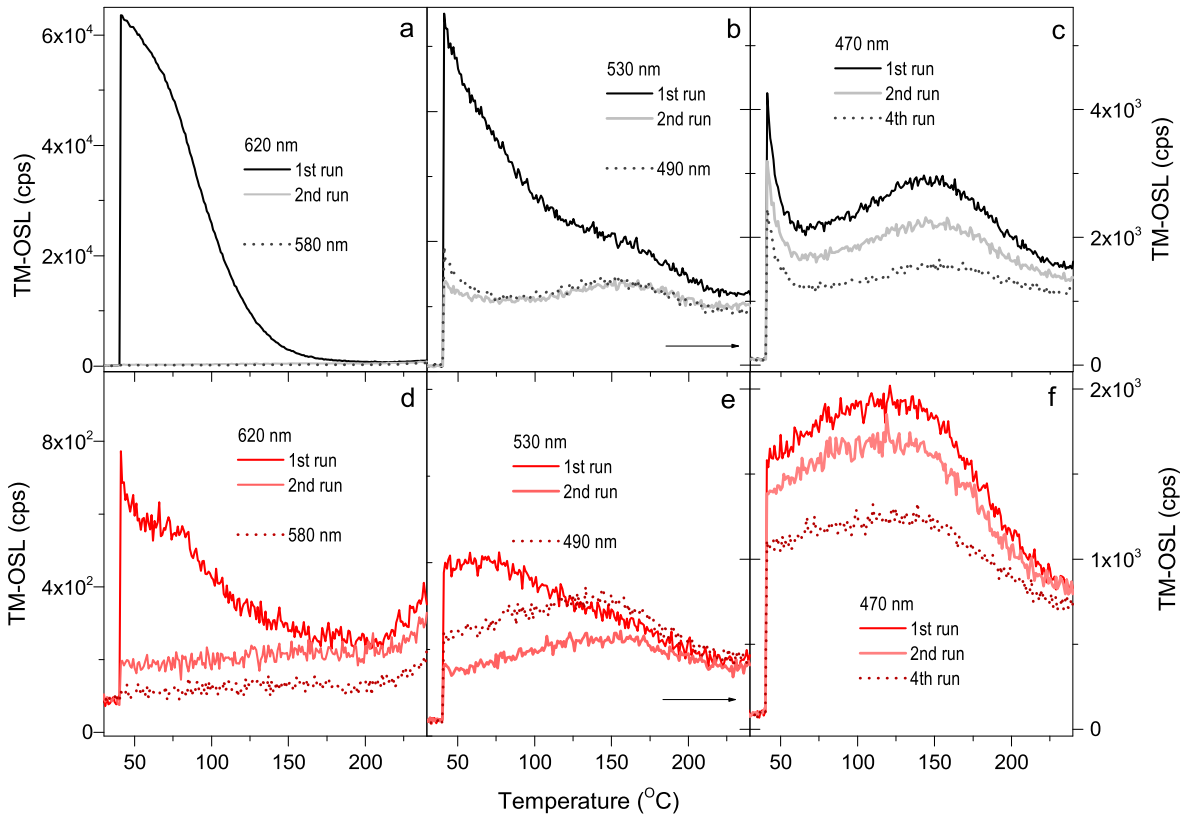

Fig. 6. TM-OSL curves for sample FB (top of the figure) and MR (bottom of the figure) were measured one after the other with indicated wavelengths after a single excitation with a dose of 300 Gy and preheat to 260 °C. Each optical stimulation was carried out during heating from 40 °C to 240 °C with a rate of 1 K s^{-1} and a photon flux density of 5.3 × 10^{17} cm^{-2} s^{-1}. The slow heating and the maximal photon flux density achievable for each LED module were used for an effective optical emptying with a particular wavelength before the next wavelength was used. Photon flux densities for different diodes (cm^{-2} s^{-1}); 620 nm - 5.3 × 10^{17}; 580 nm - 3.9 × 10^{16}; 530 nm - 1.7 × 10^{17}; 490 nm - 1.3 × 10^{17}; 470 nm - 1.0 × 10^{17}. (System 1, sample masses: FB – 5.3 mg, MR – 3.1 mg).

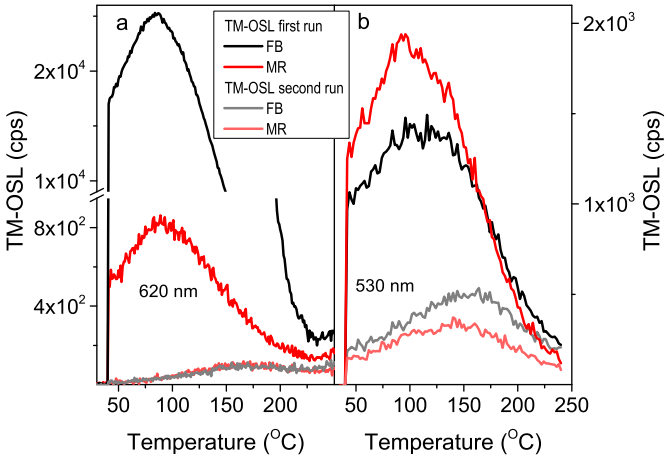

Fig. 7. (a) TM-OSL curves of samples FB and MR measured with settings optimised to separate the fast component (stimulation at 620 nm) and (b) the next in order of decay rate (stimulation at 530 nm). $TM\text{-}OSL_{620}$ was obtained during heating to 290 °C (1 K s^{-1}) and a photon flux density of 1.5 × 10^{17} cm^{-2} s^{-1}; and for $TM\text{-}OSL_{530}$ during heating to 240 °C (2 K s^{-1}) and a photon flux density of 6.7 × 10^{16} cm^{-2} s^{-1}. The outcome of the repetition of the same TM-OSL measurement carried out directly after the first run is presented in both cases. A dose of 100 Gy was administered before initial preheating to 290 °C (2 K s^{-1}). (System 2, sample masses: FB – 5.3 mg, MR – 4.8 mg)

respectively. They were measured after the same thermal treatment used for depleting the fast or both the fast and the medium components during the corresponding TM-OSL runs. Fig. 8 presents all four LM-OSL

Table 3
Protocols used in the experiment whose results are presented in Fig. 8.

Treatment		
Step	Measuring curves LM_1 and LM_2	Measuring curves LM_3 and LM_4
1	Heating to 500 °C; irradiation (150 Gy)	Heating to 500 °C; irradiation (150 Gy)
2	Preheat up to 260 °C (2 K s^{-1})	Preheat up to 260 °C (2 K s^{-1})
3	Heating to 240 °C (1 K s^{-1})	Heating to 240 °C (1 K s^{-1}) – repeated 3 times
4	LM-OSL - 5000 s, 470 nm, at 125 °C (**curve LM_1**)	LM-OSL - 5000 s, 470 nm, at 125 °C (**curve LM_3**)
5	Heating to 500 °C; irradiation (150 Gy)	Heating to 500 °C; irradiation (150 Gy)
6	Preheat up to 260 °C (2 K s^{-1})	Preheat up to 260 °C (2 K s^{-1})
7	TM-OSL - 620 nm, heating to 240 °C (1 K s^{-1})	TM-OSL - 620 nm, heating to 240 °C (1 K s^{-1})
8	LM-OSL - 5000 s, 470 nm, at 125 °C (**curve LM_2**)	TM-OSL - 530 nm, heating to 240 °C (1 K s^{-1}) - repeated 2 times
9		LM-OSL - 5000 s, 470 nm, at 125 °C (**curve LM_4**)

curves obtained for each one of the samples FB and MR. In the case of sample FB, a significant intensity decrease and a noticeable shift to longer stimulation times (from 35 s to 67 s) were observed for the first maximum of the LM-OSL curve after $TM\text{-}OSL_{620}$ (curve LM_2). The changes in the first LM-OSL maximum are much less considerable for sample MR. Here, the first maximum intensity is initially more than 33 times lower than in LM-OSL of sample FB, and after $TM\text{-}OSL_{620}$, it decreases by 40%. The shift of maximum intensity towards longer times is hardly seen. The position of the first LM-OSL maximum after $TM\text{-}OSL_{620}$

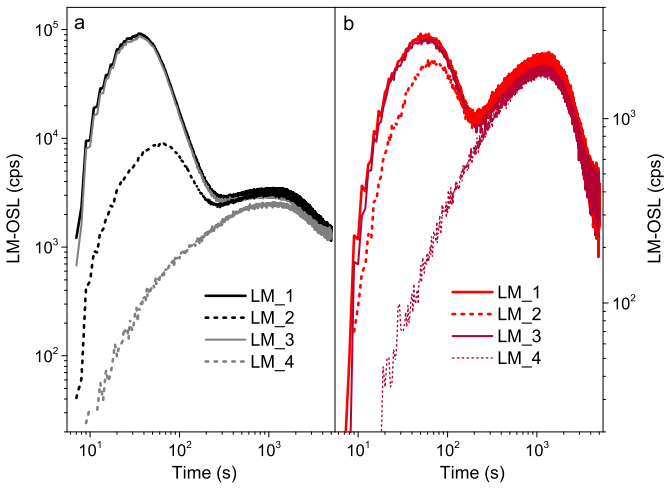

Fig. 8. Effect TM-OSL$_{620}$ and TM-OSL$_{530}$ on the shape of the LM-OSL curve of sample FB (a) and MR (b). Curves LM_1 and LM_3 were measured after the same thermal treatment applied when measurements resetting the fast (TM-OSL$_{620}$) and medium (TM-OSL$_{530}$) OSL components were realised before readout of the LM_2 and LM_4 curves, respectively. Details of the experiment are given in the text. (System 1, sample masses: FB – 4.8 mg, MR – 4.8 mg).

(curves LM_2) is the same in both samples (67 s), although in the sample MR this maximum is more than four times less intense than in FB. The shift of the time/position corresponding to maximum intensity and the full width at half maximum strongly confirms that the first bell-shaped maximum of the signal in both samples is the superimposition of different components. After TM-OSL$_{620}$ and TM-OSL$_{530}$, the first LM-OSL peak vanishes in both samples, while the second "bell" of the LM-OSL signal remains unchanged (curves LM_4). This signal is dominated by slow components, consisting of a hard-to-bleach accumulated signal with TM-OSL$_{470}$ (Fig. 6).

The combined use of both LM-OSL and TM-OSL allows for a more efficient separation of the individual components in an OSL curve. With noticeable differences in the shape of the curves obtained in both samples, the LM-OSL measurements show two separated complex maxima. On the other hand, in the TM-OSL measurements, in both samples, a significant difference was observed in the energy of stimulation photons sufficient to effectively erase the fastest component (2.0 eV/620 nm) and the next component in terms of decay rate (2.34 eV/530 nm). Another jump in the intensity of the TM-OSL signal, similar in both samples, occurs when using the wavelength of 470 nm (2.64 eV). The fast component, which can be effectively stimulated in TM-OSL measurements at 620 nm, and the medium component, for which one needs to use a wavelength as much as 90 nm shorter, form the first maximum in the LM-OSL curve, separated from the second one related to the slowest OSL components in both samples.

All curves measured in the described experiments were decomposed into individual LM-OSL components by fitting the sum of general-order-kinetics LM-OSL curves. The fitting was performed using the software package MS Excel™ with the Solver add-in utility [35,36]. The transformed original Bulur equation [14] was used, following the appropriate transformation by Polymeris et al. [37], in order to calculate the general-order LM-OSL curves. The background (BGK) signal during stimulation was included in the fitting analysis according to Ref. [38]. Frequently, the linearity is not perfect for most commercial luminescence readers at the beginning of the stimulation. In order to correct for this lack of linearity, a negative OSL component (correction curve in Fig. 9a and b) was included in the signal analysis [39]. The fit quality was tested using the Figure of Merit (FOM). In all cases, the obtained FOM values were less than 1.5%. As a result of the deconvolution analysis, the detrapping probability λ was obtained [14]. It is related to the OCS (σ) according to the formula $\lambda = I_0\sigma$, were I_0 is the density of photon flux used for stimulation.

Examples of the decomposition are shown in Fig. 9a and b, and the whole data resulting from the analysis are summarized in Fig. 9c. As the material subjected to study is quartz, the prevalence of first order of kinetics was also revealed by the deconvolution analysis. Here, each part presents results of fitting to the series of LM-OSL curves: LM_1, LM_2, LM_3, LM_4; for one aliquot. All OSC values are normalized to the OCS value obtained for the fast component in sample FB. The data show that the OCSs of individual components agree in both samples. Their values slightly deviate, when curves with different initial trap filling are compared. For sample FB, the fast component is totally erased by TM-OSL with 620 nm, and the next one, in both samples, by the TM-OSL measurement with 530 nm.

4.2.4. TR-OSL

TR-OSL measurements can provide information on the characteristics of luminescence centres involved in luminescence production in a specific window of emission wavelengths. This method records the arrival time of photons at the detector relative to the start or stop of an optical stimulation pulse, giving a cumulative spectrum of arrival times. It has been shown experimentally that the excitation time of a trapped electron and its transportation in non-localized bands after its release from the trap is much shorter than the characteristic relaxation time τ of the excited luminescence centre after capturing the electron [3, 40].

The recorded TR-OSL spectra can be approximated by two (FB) or three (MR) exponentially decaying components (Fig. 10). The component with the most prolonged decay constant in both cases probably represents a combination of the instrumental background (mostly scattered excitation light) and a signal component with a lifetime in the ms to s range [41]. Sample FB shows the well-known principal lifetime component in quartz (e.g., Ref. [42]), here ranging between 39 ± 1 μs and 42 ± 2 μs for the three analysed aliquots. Sample MR yields this component as well (~39 μs) but additionally also a shorter lifetime of the order of 4 μs (Table 4). Such lifetime components were earlier observed for low-sensitivity quartz from crystalline bedrock [43].

The general observation of much greater OSL sensitivity of FB compared to MR is confirmed by registered TR-OSL intensities, considering that the regeneration dose received by the latter is 16 times as large as the one delivered to FB (Fig. 10). Due to the dwell time of 10 μs, the short lifetime component of ~0.2 μs detected for sample FB in a previous study [7] was not observed with the experimental setup.

4.3. RL

Radioluminescence spectra of both samples were measured to investigate the luminescence centres participating in the luminescence processes. The spectra of sample FB were measured for one aliquot prepared as described in Sec. 2. This is after annealing at 490 °C for 30 min, and for another aliquot, which was not annealed. In the case of sample MR, one aliquot was measured according to the protocol listed in Table 5.

The RL spectra of the reference samples 2.2differ significantly. However, the spectrum of the MR sample becomes utterly consistent in shape with the spectrum of the FB sample after applying annealing to 480 °C (step 2, Table 5) after the first series of RL measurements (step 1, Table 5). Hence, the RL spectrum for sample MR obtained before annealing is compared with that measured for the portion of the FB sample that was not annealed to 490 °C (Fig. 11).

Shapes of the spectra differ, specifically for energies above 3 eV. Below this value, the spectra differ in intensity, but both exhibit a narrow band at 1.9 eV and then slowly increasing signals for >2.2 eV. In the range >3 eV, sample FB has the most intense signal at 3.25 eV, whereas sample MR emits a broad band between 2.5 eV and 3.5 eV with a maximum at ~2.9 eV. Above 3.5 eV, the RL intensity of sample FB decreases monotonically while sample MR has an emission band with a maximum at 3.9 eV dominating the whole spectrum. Both spectra

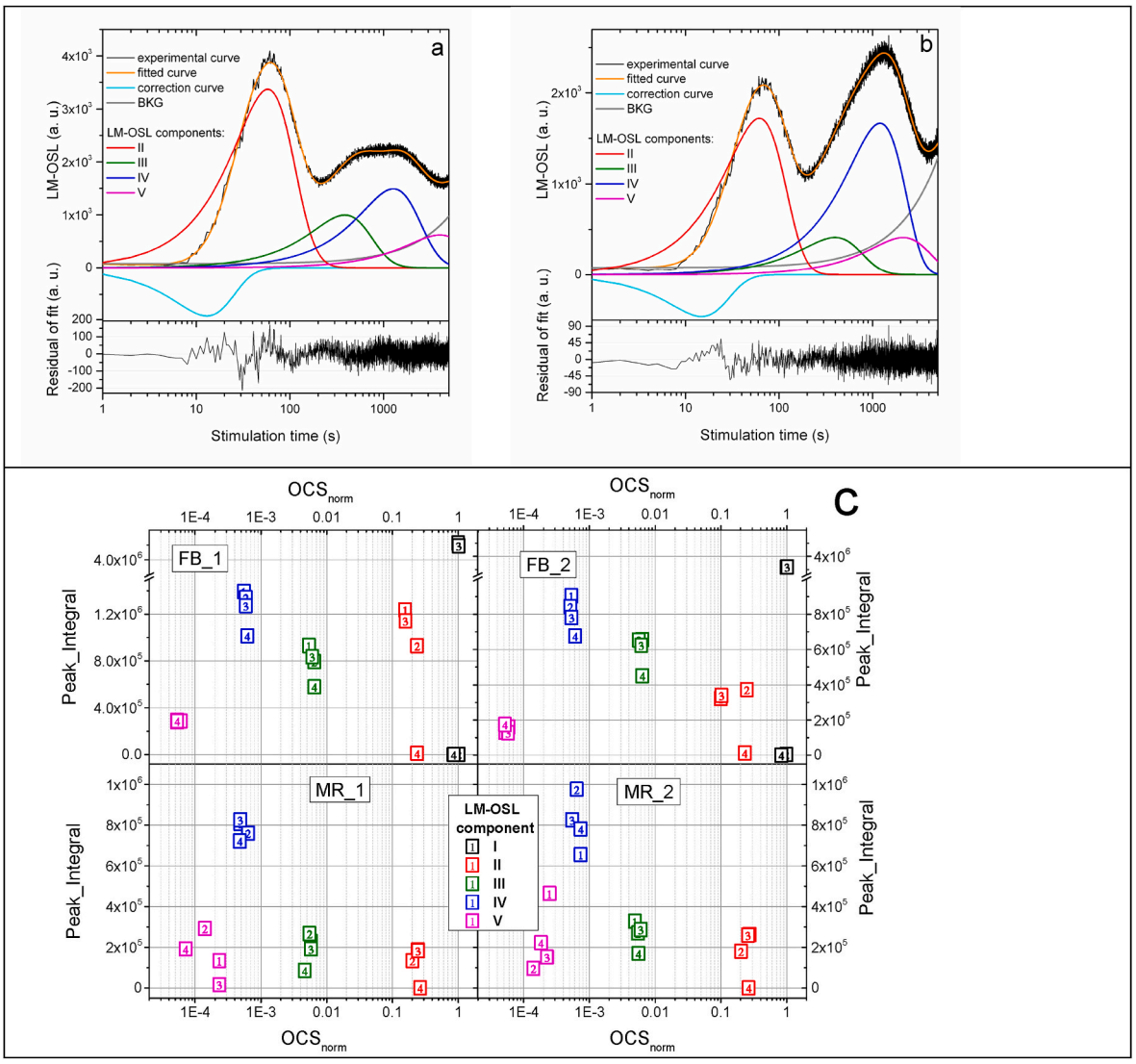

Fig. 9. Results of fitting the sum of general order kinetics LM-OSL curves to the curves measured using the sequence from Table 3. Examples of fitted LM-OSL curves for sample FB (a) and MR (b). Summary of all analysis results for two weights of each sample (c). Each point in the graphs represents a single component (each has another colour) with the specific OCS and intensity measured by the integral under the corresponding LM-OSL peak. Successive numbers in point symbols indicate successively measured LM-OSL curves: LM_1, LM_2, LM_3, LM_4 (see Table 3). The OSC values are normalized to the OCS value for the fastest component in the FB sample. (System 1, sample masses: FB_1 – 4.8 mg, FB_2 – 5.3 mg, MR_1 – 3.1 mg, MR_2 – 4.8 mg).

change during irradiation, but they behave differently. The most intense bands of sample FB decrease with dose by a factor of ~1.5–2 throughout the sequence of RL scans. In sample MR, the intense band at 3.9 eV is stable, but the emissions around 3.25 eV and 1.9 eV increase significantly by a factor of ~2.

Furthermore, the RL spectra of both samples change drastically after annealing. The initial treatment of the samples was not the same, but both underwent heating to similar temperatures, 490 °C and 480 °C for the samples FB and MR, respectively. Fig. 12 shows spectra very similar in shape. One band at 3.4 eV, which decreases significantly during irradiation, dominates all earlier seen bands. Fig. 13 compares the last spectrum recorded for samples FB and MR not annealed (Fig. 11a and b) with the first one obtained for samples after annealing (Fig. 12a and b) to show the increase in the intensity of the spectra caused by the heating. Continuous X-ray irradiation with an accumulative dose of ~400 Gy quenches the 3.4 eV emission band by factors of ~4 and ~3 for samples FB and MR but upholds the dominance of band 3.4 eV.

5. Discussion

5.1. Reference samples and standardized procedures for quartz luminescence sample characterisation

Our study introduces the new reference sample Morar (MR) in addition to and for comparison with reference sample FB that was already proposed earlier. Serving as a reference in the work of other groups, basic luminescence characterisation was performed for both samples. Most of these experiments can be repeated easily for other samples in any laboratory, allowing a direct comparison of unknown and reference samples. Such tests include TL and LM-OSL measurements and a sequence for recording sensitivity changes of the 110 °C TL peak with accumulated dose. Whereas TL and OSL measurements target the domain of thermally and optically sensitive electron traps, the measurement of sensitivity changes is the most straightforward test available using a standard TL/OSL reader that relates to changes in the filling of luminescence centres. Details about these three basic experiments and obtained results for the reference samples are included in the supplementary material.

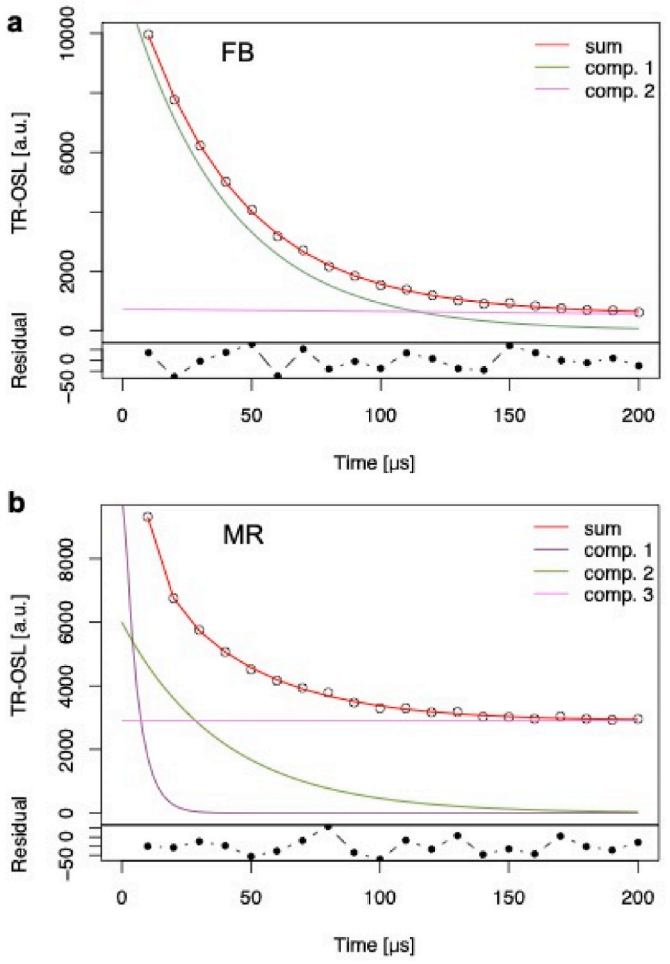

Fig. 10. Typical TR-OSL spectra for one aliquot of samples FB (a) and MR (b). The fitted lifetime components are shown in green and purple. The instrumental background as fitted by the algorithm is indicated in pink. See the text for further details on the measurement parameters.

Table 4
TR-OSL lifetime components for the FB and MR samples.

Aliquot	FB	MR	
	τ_1 [µs]	τ_1 [µs]	τ_2 [µs]
1	39 ± 1	3.9 ± 0.9	39 ± 5
2	41 ± 1	–	–
3	42 ± 2	4.1 ± 2.0	38 ± 10

Table 5
Applied radioluminescence sequence.

Step	Treatment
1	RL measurements under continuous X-ray irradiation (20 min, ~400 Gy total)
2	TL up to 480 °C (1 K s^{-1})
3	RL measurements under continuous X-ray irradiation (20 min, ~400 Gy total)
(4)	(TL up to 480 °C (1 K s^{-1}))

Despite the fact that some data scatter related to individual instruments and their calibration is expected (cf. [6]), standardised sample characterisation sequences indubitably allow a more objective assessment of a sample's luminescence properties. In addition, reference samples with approved physical characteristics could be used to check the performance of luminescence equipment. For example, the principal lifetime component identified in TR-OSL experiments for both the FB and the MR samples might help test the performance of other instruments relative to the one used for initial sample characterisation.

In view of luminescence sensitization studies (e.g., Refs. [44,45]), recently developed approaches of provenance analyses using the luminescence signals of quartz (and feldspar; e.g., Refs. [46–48]) or explorative luminescence data analysis [49], standardized datasets as proposed here will prove essential to facilitate valid comparisons across samples.

Finally, accurate documentation of all laboratory treatments undergone by the reference samples is crucial. Unfortunately, the sample's true history is usually unknown for natural minerals before it was collected and purified, thus hampering a direct comparison of luminescence properties. We have only vague ideas about the number of sedimentary cycles, any thermal exposure (e.g., wildfires) or the cumulative radiation dose received by the samples. In our case, one of the samples (FB) was annealed in the laboratory, while sample MR was not (yet) subject to any heat treatment. Although this difference might, at first sight, complicate the comparison of results between the two datasets, there is still the possibility to study the change in luminescence characteristics induced by heat treatments because unannealed FB material is available for this purpose (cf. Sec. 4.3).

5.2. *Reference sample properties in relation to previous studies*

In terms of TL signatures, the FB and MR reference samples show 4–5 peaks visible in the bulk TL glow curve (recorded in the UV emission window; Fig. 1) that are frequently recorded also for other natural and synthetic quartz samples [1,50,51]. Despite the differences in the shape of the TL curves of both samples as a function of dose, one can infer that they do not indicate different types of traps in the samples but rather differences in the concentration of defects associated with the traps. The modelling seems to support this conclusion. An exception might be the TL in the range 150–250 °C, where the two samples depict a non-congruent pattern of TL maxima. The TL properties of samples FB and MR cover at least part of the variability expected for various types of quartz but do not demand a fundamentally new understanding.

The very weak fast OSL component in sample MR compared to its intense occurrence in sample FB reflects well the differences in OSL signal composition among natural samples from various environments and geological history. Low-sensitivity quartz has, for instance, been described in Preusser et al. [52] and Klasen et al. [53], while a more comprehensive survey of OSL signal composition as a function of lithology, weathering and transport history was presented by Jeong and Choi [54]. Intriguingly, many studies emphasize the importance of sedimentary cycling to sensitise the quartz OSL signal (and the fast component in particular; [55–57]), while sample MR is almost devoid of the fast component and low in sensitivity despite presumably many depositional cycles undergone during its fluvial and littoral history. On the other hand, sample FB might represent quartz from environments in which many (aeolian) depositional cycles sensitized the fast component (e.g., old deserts), thus potentially rendering them more suitable for dating purposes (e.g., Refs. [58,59]).

The TR-OSL signal of both reference samples contains the principal lifetime component observed for most natural quartz samples [42]. The observation of shorter lifetime components in sample MR makes it a candidate to study their origin, given that a more extensive set of complementary analytical data will be available for this sample, allowing the correlation of short lifetimes with TL, OSL and RL characteristics as well as with previous TR-OSL investigations (e.g., Refs. [7,43]).

All bands recognizable in the RL spectra of the FB and MR samples are known from previous RL studies of quartz. For example, the RL band at 3.4 eV, dominant in the signal of both samples heated to 480 °C or 490 °C (Fig. 12), was previously observed in synthetic quartz (C band; [60]) and natural quartz [61], for which a substantial increase in intensity was also reported after annealing to 500 °C and prior irradiation.

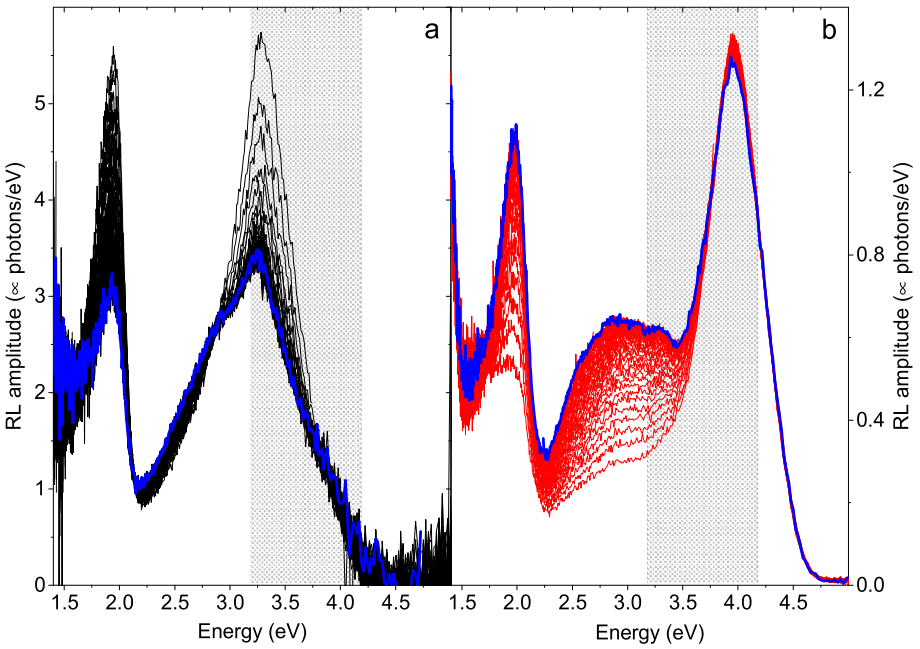

Fig. 11. Radioluminescence spectra of a batch of sample FB that did not undergo the last step of the preparation (annealing to 490 °C) (a) and spectra of sample MR as received (b). The last spectrum in the series of measurements is marked in blue. The spectral detection range applied in TL, and LM-OSL measurements is indicated in grey. Sample masses are about 20 mg.

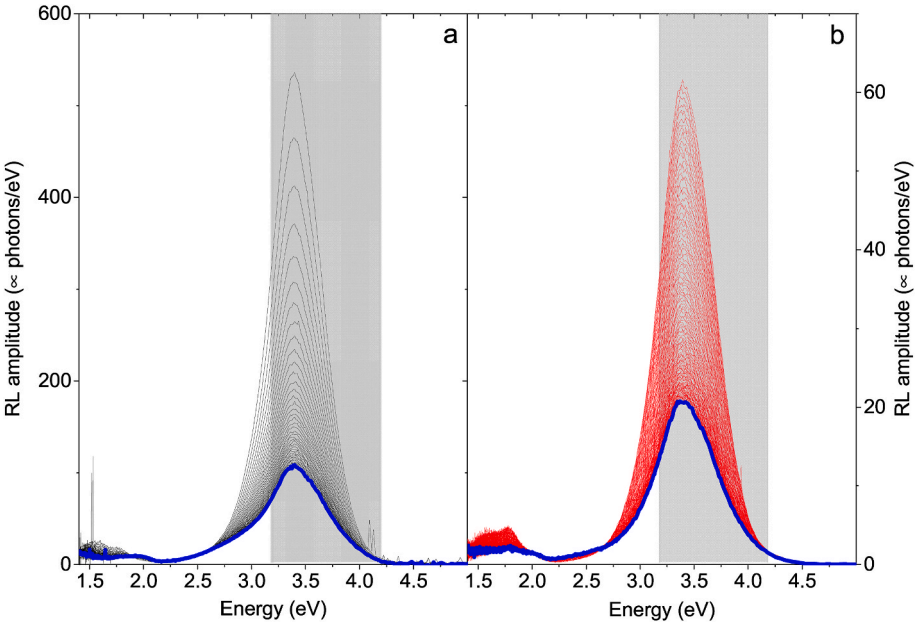

Fig. 12. Radioluminescence spectra of sample FB as received (a) and MR after the TL measurement up to 480 °C (2 K s^{-1}) (b). The last spectrum in the series of measurements is marked in blue. The spectral detection range applied in TL, and LM-OSL measurements is indicated in grey. Sample masses are about 20 mg.

Such a signal increase was, as here, followed by a gradual decrease in the intensity in subsequent measurements of the RL spectrum until a stable level was reached [62]. In this study, the 3.4 eV band seems to be identical to the 3.25 eV band seen very clearly in the spectra of sample FB before the anneal at 490 °C, but also noticeable in the spectra of the untreated MR sample (Fig. 11). In unannealed sample FB, this band decreases with progressive RL measurements. It is worth mentioning that a band at 3.3 eV was observed in cathodoluminescence (CL) spectra measured for synthetic quartz, and a similar decrease of the band intensity under the electron beam was noted [63]. The low energy band at 1.9 eV, as well as that of the highest energy, at 3.9 eV, observed in sample MR before heating appears in both the RL (band O in Pagonis et al. [61]) and CL studies [63–65]. Another band between 2.5 eV and 2.9 eV, known from literature on quartz RL and CL, can also be seen in the RL of both samples before heating.

The RL measurements show that the samples differ more in the concentration of luminescent centres than in their types, which was already indicated by the modelling of the TL curves. The exception is the 3.9 eV band (reported in Ref. [66]), which is observed in the MR sample but is absent in sample FB. Based on the presented results, one can conclude that both samples are a good representation of natural quartz, and it is not necessary to introduce a new type of centre, not recognized

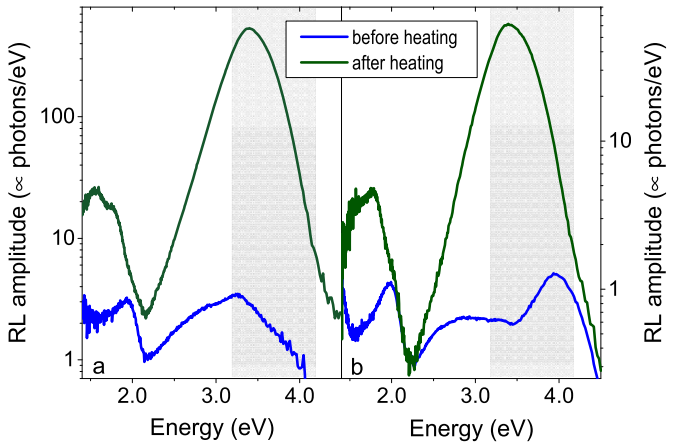

Fig. 13. A comparison of the spectrum obtained as the last one in the series presented in Fig. 11, with the first spectrum of the series shown in Fig. 12 for sample FB (a) and sample MR (b). The spectral detection range applied in TL and LM-OSL measurements is indicated in grey.

earlier, to describe the phenomena occurring in them.

Whereas TL, LM-OSL and TM-OSL target the electron trapping sites, TR-OSL and the acquired RL spectra offer information on the recombination centres involved in luminescence production. The latter two methodologies require special equipment not available in most routine laboratories for dosimetry and dating. From a practical perspective, it is hence more straightforward to characterize the electron traps, as reflected in the proposed standardized sample characterisation procedures (see supplementary material). Nonetheless, spectrometric techniques should be part of any luminescence sample screening. An improved understanding of charge dynamics related to luminescence properties can only be achieved through the combination of analyses directed at the traps and the recombination centres (cf. [67]).

5.3. Future directions

The initial results obtained here can only be the first step of a series of more specialized experiments to further characterize the physical and chemical properties of the reference samples. For instance, as the TL and OSL data presented here were mainly acquired in a monochromatic mode, future efforts will include detailed spectrometric TL and OSL analyses of both samples, including spectrally-resolved dose-response of individual emissions (to be published in an upcoming study). Likewise, the dose evolution of individual components of the OSL signal as extracted by decomposition approaches will offer new insights into sample characteristics.

Finally, determining absolute physical parameters describing the luminescence processes in the reference samples will further help us refine the existing quartz models. Such parameters include the thermal stability (expressed as trap depth E (eV) and frequency factor s (s^{-1})) and the optical sensitivity (expressed as photoionization cross-section) of individual signal components (i.e., electron traps associated with certain TL and OSL components). For these efforts, it is paramount to ensure accurate sample temperature control and photon flux for optical stimulation.

6. Conclusions

Proper understanding of luminescence production in quartz requires experiments on suitable, well-studied reference samples for reproducible results. We applied multiple luminescence techniques (TL, OSL, LM-OSL, TM-OSL, TR-OSL, and RL) on two reference samples (FB and MR). Both samples consist of >99% SiO_2. TL intensities of both samples differ by factors of 2 (110 °C peak) to 26 (200 °C peak), and TL curves >150 °C show pronounced maxima at 185 °C and 285 °C for FB and 165 °C and 250 °C for MR. TL dose response in different glow curve regions varies across the two samples, i.e., with increasing filling of deep electron traps. The OSL fast component is 80 times, and the next component in terms of the decay rate (medium component) above four times more intense in the FB sample than in MR. The intensities of the slow components creating the second LM-OSL maximum are comparable in their intensities in both samples. TM-OSL curve shapes differ most with stimulation at 530 nm after complete quenching of the fast component. The slow component intensity in 470 nm TM-OSL measurements is similar in both samples, but rapid signal decay is visible only for the FB sample. Luminescence signal behaviour with increasing dose indicates different competition between centres and traps in both samples. That, in turn, is a sign of substantial differences between the two samples in terms of defect concentrations rather than different types involved in the luminescence process. This finding seems to be supported by the RL measurements and our modelling. Such apparent diversity offers a chance to constrain better the variability of expected defect concentrations in natural samples.

Authors contribution

CS initiated the manuscript and carried out TR-OSL measurements. ACh organised the write-up of the manuscript and, together with MB, performed TL, LM-OSL and TM-OSL measurements. MF and MM were responsible for the RL measurements. GSP was our LM-OSL specialist. SK helped with the TR-OSL analysis, modelled quartz signals, and validated the LM-OSL data. DCWS, ACr and GA contributed to interpreting the results and manuscript editing. All authors contributed to the discussion and the writing of the manuscript.

Data availability

The raw data from this study are available via Zenodo: Schmidt, S., Chruścińska, A., Fasoli, M., Biernacka, M., Kreutzer, S., Polymeris, G.S., Sanderson, D.C.W., Cresswell, A., Adamiec, G., Martini, M., 2022. Dataset: A systematic multi-technique comparison of luminescence characteristics of two reference quartz samples. (1.0) [Data set]. Zenodo. https://doi.org/10.5281/zenodo.6325144.

Declaration of competing interest

The authors declare that they have no known competing financial interests or personal relationships that could have appeared to influence the work reported in this paper.

Acknowledgements

In 2021/2022, when this manuscript was written, SK received funding from the European Union's Horizon 2020 research and innovation programme under the Marie Skłodowska-Curie grant agreement No. 844457 (CREDit). MB did the experiments using the equipment belonging to the Centre for Modern Interdisciplinary Technologies, Nicolaus Copernicus University in Torun, ul. Wilenska 4, 87–100 Torun, Poland (e-mail: icnt@umk.pl) and has been financed by the grant of the National Science Centre, Poland, No. 2018/31/B/ST10/03917.

Appendix A. Supplementary data

Supplementary data to this article can be found online at https://doi.org/10.1016/j.jlumin.2022.119070.

References

[1] F. Preusser, M.L. Chithambo, T. Götte, M. Martini, K. Ramseyer, E.J. Sendezera, G. J. Susino, A.G. Wintle, Quartz as a natural luminescence dosimeter, Earth Sci. Rev. 97 (2009) 184–214, https://doi.org/10.1016/j.earscirev.2009.09.006.

[2] A. Kronz, A.M. Van den Kerkhof, A. Müller, Analysis of low element concentrations in quartz by electron microprobe, in: J. Götze, R. Möckel (Eds.), Quartz: Deposits, Mineralogy and Analytics, Springer, Berlin, 2012, pp. 191–217.

[3] R. Chen, V. Pagonis, Thermally and Optically Stimulated Luminescence - a Simulation Approach, John Wiley & Sons, Ltd, 2011.

[4] R. Chen, V. Pagonis, Advances in Physics and Applications of Optically and Thermally Stimulated Luminescence, World Scientific (Europe), 2019.

[5] S. Kreutzer, J. Friedrich, D. Sanderson, G. Adamiec, A. Chruścińska, M. Fasoli, M. Martini, G. Polymeris, C. Burbidge, C. Schmidt, Les sables de Fontainebleau: a natural quartz reference sample and its characterisation, Ancient TL 35 (2017) 21–37 (hal-01846142).

[6] C. Schmidt, J. Friedrich, G. Adamiec, A. Chruścińska, M. Fasoli, S. Kreutzer, M. Martini, L. Panzeri, G.S. Polymeris, K. Przegiętka, P.G. Valla, G.E. King, D.C. W. Sanderson, How reproducible are kinetic parameter constraints of quartz luminescence? An interlaboratory comparison for the 110 °C TL peak, Radiat. Meas. 110 (2018) 14–24, https://doi.org/10.1016/j.radmeas.2018.01.002.

[7] C. Schmidt, O. Simmank, S. Kreutzer, Time-resolved optically stimulated luminescence of quartz in the nanosecond time domain, J. Lumin. 213 (2019) 376–387, https://doi.org/10.1016/j.jlumin.2019.05.042.

[8] A. Chruścińska, A. Szramowski, Thermally modulated optically stimulated luminescence (TM-OSL) of quartz, J. Lumin. 195 (2018) 435–440, https://doi.org/10.1016/j.jlumin.2017.12.004.

[9] A. Chruścińska, A. Szramowski, Thermally modulated OSL related to the fast component of the OSL signal in quartz, Radiat. Meas. 120 (2018) 20–25, https://doi.org/10.1016/j.radmeas.2018.05.011.

[10] J. Friedrich, M. Fasoli, S. Kreutzer, C. Schmidt, On the dose rate dependence of radiofluorescence signals of natural quartz, Radiat. Meas. 111 (2018) 19–26, https://doi.org/10.1016/j.radmeas.2018.02.006.

[11] J. Friedrich, S. Kreutzer, C. Schmidt, Making the invisible visible: observing the UV-reversal effect in quartz using radiofluorescence, J. Phys. D Appl. Phys. 51 (33) (2018), 335105, https://doi.org/10.1088/1361-6463/aacfd0.

[12] J. Friedrich, S. Kreutzer, C. Schmidt, Radiofluorescence as a detection tool for quartz luminescence quenching processes, Radiat. Meas. 120 (2018) 33–40, https://doi.org/10.1016/j.radmeas.2018.03.008.

[13] British Geological Survey, 1:63,360/1:50,000 geological map series, sheet 61 (Arisaig), Geological Survey of Scotland (1971) (Nottingham).

[14] E. Bulur, An alternative technique for optically stimulated luminescence (OSL) experiment, Radiat. Meas. 26 (1996) 701–709, https://doi.org/10.1016/S1350-4487(97)82884-3, 1996.

[15] D. Richter, A. Richter, K. Dornich, Lexsyg — a new system for luminescence research, Geochron 40 (2013) 220–228, https://doi.org/10.2478/s13386-013-0110-0.

[16] R. Galloway, Luminescence lifetimes in quartz: dependence on annealing temperature prior to beta irradiation, Radiat. Meas. 35 (2002) 67–77, https://doi.org/10.1016/S1350-4487(01)00258-X.

[17] R Core Team, R: A Language and Environment for Statistical Computing, 2022. https://www.r-project.org. (Accessed 4 March 2022).

[18] S. Kreutzer, C. Schmidt, M.C. Fuchs, M. Dietze, M. Fischer, M. Fuchs, Introducing an R package for luminescence dating analysis, Ancient TL 30 (2012) 1–8, hdl: 10013/epic.44194.

[19] S. Kreutzer, C. Burow, M. Dietze, M.C. Fuchs, C. Schmidt, M. Fischer, J. Friedrich, N. Mercier, A. Philippe, S. Riedesel, M. Autzen, D. Mittelstrass, H.J. Gray, J. Galharret, Luminescence: Comprehensive Luminescence Dating Data Analysis, 2021. R package version 0.9.16, https://CRAN.R-project.org/package=Luminescence. (Accessed 4 March 2022).

[20] J. Friedrich, V. Pagonis, R. Chen, S. Kreutzer, C. Schmidt, Quartz radiofluorescence: a modelling approach, J. Lumin. 186 (2017) 318–325, https://doi.org/10.1016/j.jlumin.2017.02.039.

[21] R.M. Bailey, Towards a general kinetic model for optically and thermally stimulated luminescence of quartz, Radiat. Meas. 33 (2001) 17–45, https://doi.org/10.1016/S1350-4487(00)00100-1.

[22] J. Friedrich, S. Kreutzer, C. Schmidt, Solving ordinary differential equations to understand luminescence: "RLumModel" an advanced research tool for simulating luminescence in quartz using R, Quat. Geochronol. 35 (2016) 88–100, https://doi.org/10.1016/j.quageo.2016.05.004.

[23] G. Kitis, V. Pagonis, Computerized curve deconvolution analysis for LM-OSL, Radiat. Meas. 43 (2008) 737–741, https://doi.org/10.1016/j.radmeas.2007.12.055.

[24] G.S. Polymeris, G. Kitis, N.C. Tsirliganis, Correlation between TL and OSL properties of CaF2:N, Nucl. Instrum. Methods B. 251 (2006) 133–142, https://doi.org/10.1016/j.nimb.2006.05.023.

[25] N.A. Spooner, On the optical dating signal from quartz, Radiat. Meas. 23 (1994) 593–600, https://doi.org/10.1016/1350-4487(94)90105-8.

[26] G.I. Dallas, G.S. Polymeris, D. Afouxenidis, N.C. Tsirliganis, N.F. Tsagas, G. Kitis, Correlation between TL and OSL signals in KMgF3:Ce3+: bleaching study of individual glow-peaks, Radiat. Meas. 45 (2010) 537–539, https://doi.org/10.1016/j.radmeas.2009.11.008.

[27] V. Angeli, G.S. Polymeris, I.K. Sfampa, N.C. Tsirliganis, G. Kitis, Component resolved bleaching study in natural calcium fluoride using CW-OSL, LM-OSL and residual TL glow curves after bleaching, Appl. Radiat. Isot. 122 (2017) 89–95, https://doi.org/10.1016/j.apradiso.2017.01.014.

[28] Ş. Kaya-Keleş, G.S. Polymeris, N. Meriç, A component resolved study on the stable signal of Merck α-quartz: tentative correlation among TL peaks, OSL components and EPR signals, Nucl. Instrum. Methods B. 458 (2019) 44–56, https://doi.org/10.1016/j.nimb.2019.07.029.

[29] A.G. Wintle, Thermal quenching of thermoluminescence in quartz, Geophys. J. Roy. Astron. Soc. 41 (1975) 107–113, https://doi.org/10.1111/j.1365-246X.1975.tb05487.x.

[30] R. Nanjundaswamy, K. Lepper, S.W.S. McKeever, Thermal quenching of thermoluminescence in natural quartz, Radiat. Prot. Dosim 100 (2002) 305–308, https://doi.org/10.1093/oxfordjournals.rpd.a005874, 2002. Thermal quenching of thermoluminescence in natural quartz.

[31] B. Subedi, E. Oniya, G.S. Polymeris, D. Afouxenidis, N.C. Tsirliganis, G. Kitis, Thermal quenching of thermoluminescence in quartz samples of various origin, Nucl. Instrum. Methods Phys. Res. B. 269 (2011) 572–581, https://doi.org/10.1016/j.nimb.2011.01.011.

[32] A. Chruścińska, N. Kijek, Thermally modulated optically stimulated luminescence (TM–OSL) as a tool of trap parameter analysis, J. Lumin. 174 (2016) 42–48, https://doi.org/10.1016/j.jlumin.2016.01.012.

[33] A. Chruścińska, N. Kijek, S. Topolewski, Recent development in the optical stimulation of luminescence, Radiat. Meas. 106 (2017) 13–19, https://doi.org/10.1016/j.radmeas.2017.01.013.

[34] A. Chruścińska, P. Palczewski, T. Rerek, Slow OSL component in quartz separated by TM-OSL method, Radiat. Meas. 134 (2020), 106316, https://doi.org/10.1016/j.radmeas.2020.106316.

[35] G. Kitis, V. Pagonis, Computerized curve deconvolution analysis for LM-OSL, Radiat. Meas. 43 (2008) 737–741, https://doi.org/10.1016/j.radmeas.2007.12.055.

[36] D. Afouxenidis, G.S. Polymeris, N.C. Tsirliganis, G. Kitis, Computerised curve deconvolution of TL/OSL curves using a popular spreadsheet program, Radiat. Protect. Dosim. 149 (2012) 363–370, https://doi.org/10.1093/rpd/ncr315.

[37] G.S. Polymeris, N.C. Tsirliganis, Z. Loukou, G. Kitis, A comparative study of the anomalous fading effects of TL and OSL signals of Durango apatite, Phys. Status Solidi A 203 (2006) 578–590, https://doi.org/10.1002/pssa.200521347, 2006.

[38] E.O. Oniya, G.S. Polymeris, N.C. Tsirliganis, G. Kitis, Radiation dose response correlation between thermoluminescence and optically stimulated luminescence in quartz, J. Lumin. 132 (2012) 1720–1728, https://doi.org/10.1016/j.jlumin.2012.02.005.

[39] G.I. Dallas, D. Afouxenidis, E.C. Stefanaki, N.F. Tsagas, G.S. Polymeris, N. C. Tsirliganis, G. Kitis, Reconstruction of the thermally quenched glow-curve of Al2O3:C, Phys. Status Solidi A 205 (2008) 1672–1679, https://doi.org/10.1002/pssa.200824016.

[40] S. Tsukamoto, A. Murray, C. Ankjærgaard, M. Jain, T. Lapp, Charge recombination processes in minerals studied using optically stimulated luminescence and time-resolved exo-electrons, J. Phys. D Appl. Phys. 43 (2010), 325502, https://doi.org/10.1088/0022-3727/43/32/325502.

[41] C. Ankjærgaard, M. Jain, Optically stimulated phosphorescence in quartz over the millisecond to second time scale: insights into the role of shallow traps in delaying luminescent recombination, J. Phys. D Appl. Phys. 43 (2010), 255502, https://doi.org/10.1088/0022-3727/43/25/255502.

[42] C. Ankjærgaard, M. Jain, K.J. Thomsen, A.S. Murray, Optimising the separation of quartz and feldspar optically stimulated luminescence using pulsed excitation, Radiat. Meas. 45 (2010) 778–785, https://doi.org/10.1016/j.radmeas.2010.03.004.

[43] M.L. Chithambo, F. Preusser, K. Ramseyer, F.O. Ogundare, Time-resolved luminescence of low sensitivity quartz from crystalline rocks, Radiat. Meas. 42 (2007) 205–212, https://doi.org/10.1016/j.radmeas.2006.07.005.

[44] L.A. Gliganic, T.J. Cohen, M. Meyer, A. Molenaa, Variations in luminescence properties of quartz and feldspar from modern fluvial sediments in three rivers, Quat. Geochronol. 41 (2017) 70–82, https://doi.org/10.1016/j.quageo.2017.06.005.

[45] T. Bartyik, G. Magyar, D. Filyó, O. Tóth, V. Blanka-Végi, T. Kiss, S. Marković, I. Persoiu, M. Gavrilov, G. Mezősi, G. Sipos, Spatial differences in the luminescence sensitivity of quartz extracted from Carpathian Basin fluvial sediments, Quat. Geochronol. 64 (2021), 101166, https://doi.org/10.1016/j.quageo.2021.101166.

[46] H.J. Gray, M. Jain, A.O. Sawakuchi, S.A. Mahan, G.E. Tucker, Luminescence as a sediment tracer and provenance tool, Rev. Geophys. 57 (2019) 987–1017, https://doi.org/10.1029/2019RG000646.

[47] A.O. Sawakuchi, M. Jain, T.D. Mineli, L. Nogueira, D.J. Bertassoli, C. Häggi, H. O. Sawakuchi, F.N. Pupim, C.H. Grohmann, C.M. Chiessi, M. Zabel, S. Mulitza, C.E. M. Mazoca, D.F. Cunha, Luminescence of quartz and feldspar fingerprints provenance and correlates with the source area denudation in the Amazon River basin, Earth Planet Sci. Lett. 492 (2018) 152–162, https://doi.org/10.1016/j.epsl.2018.04.006.

[48] A.O. Sawakuchi, F.C.G. Rodrigues, T.D. Mineli, V.R. Mendes, D.B. Melo, C. M. Chiessi, P.C.F. Giannini, Optically stimulated luminescence sensitivity of quartz for provenance analysis, Methods and Protocols 3 (1) (2020) 6, https://doi.org/10.3390/mps3010006.

[49] C. Burow, J. Zens, S. Kreutzer, M. Dietze, M.C. Fuchs, M. Fischer, C. Schmidt, H. Brückner, Exploratory Data Analyses Using the R Package 'Luminescence – towards Data Mining in OSL Applications, Poster at UK luminescence and ESR meeting, Liverpool, UK, 2016. https://doi.org/10.13140/RG.2.2.19673.62561.

[50] S.A. Petrov, I.K. Bailiff, The '110°C' TL peak in synthetic quartz, Radiat. Meas. 24 (1995) 519–523, https://doi.org/10.1016/1350-4487(95)00002-V.

[51] V. Pagonis, E. Tatsis, G. Kitis, C. Drupieski, Search for common characteristics in the glow curves of quartz of various origins, Radiat. Protect. Dosim. 100 (2002) 373–376, https://doi.org/10.1093/oxfordjournals.rpd.a005892.

[52] F. Preusser, K. Ramseyer, C. Schlüchter, Characterisation of low OSL intensity quartz from the New Zealand Alps, Radiat. Meas. 41 (2006) 871–877, https://doi.org/10.1016/j.radmeas.2006.04.019.
[53] N. Klasen, M. Fiebig, F. Preusser, U. Radtke, Luminescence properties of glaciofluvial sediments from the bavarian alpine foreland, Radiat. Meas. 41 (2006) 866–870, https://doi.org/10.1016/j.radmeas.2006.04.014.
[54] G.Y. Jeong, J.-H. Choi, Variations in quartz OSL components with lithology, weathering and transportation, Quat. Geochronol. 10 (2012) 320–326, https://doi.org/10.1016/j.quageo.2012.02.023.
[55] P. Moska, A.S. Murray, Stability of the quartz fast-component in insensitive samples, Radiat. Meas. 41 (2006) 878–885, https://doi.org/10.1016/j.radmeas.2006.06.005.
[56] T.J. Pietsch, J.M. Olley, G.C. Nanson, Fluvial transport as a natural luminescence sensitiser of quartz, Quat. Geochronol. 3 (2008) 365–376, https://doi.org/10.1016/j.quageo.2007.12.005.
[57] A.O. Sawakuchi, M.W. Blair, R. DeWitt, F.M. Faleiros, T. Hyppolito, C.C.F. Guedes, Thermal history versus sedimentary history: OSL sensitivity of quartz grains extracted from rocks and sediments, Quat. Geochronol. 6 (2011) 261–272, https://doi.org/10.1016/j.quageo.2010.11.002.
[58] K.E. Fitzsimmons, E.J. Rhodes, T.T. Barrows, OSL dating of southeast Australian quartz: a preliminary assessment of luminescence characteristics and behaviour, Quat. Geochronol. 5 (2010) 91–95, https://doi.org/10.1016/j.quageo.2009.02.009.
[59] C.M. Neudorf, O.B. Lian, P.D. McIntos, T.B. Gingerich, P.C. Augustinus, Investigation into the OSL and TT-OSL signal characteristics of ancient (>100 ka) Tasmanian aeolian quartz and its utility as a geochronometer for understanding long-term climate-driven landscape change, Quat. Geochronol. 53 (2019), 101005, https://doi.org/10.1016/j.quageo.2019.101005.
[60] M. Martini, M. Fasoli, A. GalliA, I. Villa, P. Guibert, Radioluminescence of synthetic quartz related to alkali ions, J. Lumin. 132 (2012) 1030–1036, https://doi.org/10.1016/j.jlumin.2011.11.031.
[61] V. Pagonis, M.L. Chithambo, R. Chen, A. Chruścińska, M. Fasoli, S.H. Li, M. Martini, K. Ramseyer, Thermal dependence of luminescence lifetimes and radioluminescence in quartz, J. Lumin. 145 (2014) 38–48, https://doi.org/10.1016/j.jlumin.2013.07.022.
[62] M. Martini, M. Fasoli, I. Villa, P. Guibert, Radioluminescence of synthetic and natural quartz, Radiat. Meas. 47 (2012) 846–850, https://doi.org/10.1016/j.radmeas.2012.01.008.
[63] M.A. Stevens-Kalceff, Cathodoluminescence microcharacterization of point defects in a-quartz, Mineral. Mag. 73 (2009) 585–605, https://doi.org/10.1180/minmag.2009.073.4.585.
[64] M.A. Stevens-Kalceff, M. Phillips, Cathodoluminescence microcharacterization of the defect structure of quartz, Phys. Rev. B 52 (1995), 31223134, https://doi.org/10.1103/PhysRevB.52.3122.
[65] T. Götte, K. Ramseyer, Trace element characteristics, luminescence properties and real structure of quartz, in: J. Götze, R. Möckel (Eds.), Quartz: Deposits, Mineralogy and Analytics, Springer, Berlin, 2012, pp. 265–285.
[66] M. Martini, M. Fasoli, I. Villa, Defect studies in quartz: composite nature of the blue and UV emissions, Nucl. Instrum. Methods B. 327 (2014) 15–21, https://doi.org/10.1016/j.nimb.2013.09.048.
[67] P. Bräunlich, Thermally stimulated relaxation in solids, Top. Appl. Phys. 39 (1979). Springer, Berlin.